Electrochemical synthesis of PbTe in NaOH solution

Lingling Shen[1], Wencai He[1], Aimin Liu[1], Bo Zhao[1], Ramana Reddy[2], Blanka Kubikova[3], Michal Korenko[3], Zhongning Shi[1,]*

[1] School of Metallurgy, Northeastern University, Shenyang 110819, China
[2] Department of Metallurgical and Materials Engineering, the University of Alabama, Tuscaloosa, AL 35487-0202, USA
[3] Institute of Inorganic Chemistry, Slovak Academy of Sciences, Bratislava 84536, Slovakia
[*]E-mail: znshi@mail.neu.edu.cn

Lead telluride (PbTe) was electrochemically synthesized in NaOH solution at room temperature, and the reduction mechanism of PbTe was investigated using cyclic voltammetry and chronoamperometry. The reduction of Pb(II) to Pb(0) in 5 mM $Pb(NO_3)_2$ - 100 mM NaOH solution was a one-step two-electron transfer process, while the reduction of Te(IV) to Te(0) in 10 mM TeO_2 - 100 mM NaOH solution was a one-step four-electron transfer process. PbTe deposits were obtained at a potential range from −0.95 V to −1.05 V (vs. Hg/HgO) in a mixture of 10 mM TeO_2, 5 mM $Pb(NO_3)_2$, and 100 mM NaOH solution. The nucleation mechanisms of Pb and Te were three-dimensional instantaneous and progressive nucleation, respectively. However, the nucleation mechanism of PbTe was a combination of three-dimensional instantaneous and progressive nucleation at −1.0 V (vs. Hg/HgO). The nucleation mechanisms at different potentials correspond to the dominant electrodeposited element.

1. INTRODUCTION

Lead telluride (PbTe), a kind of thermoelectric material (TE) converting energy between heat and electricity by the transport of a carrier (electron or hole) in solid materials, is often applied in the area of space, optoelectronics and medical biology. Based on the utilization condition temperature, thermoelectric materials can usually be divided into three groups including low-temperature, medium-temperature and high-temperature thermoelectric materials. PbTe is a kind of high temperatures thermoelectric materials and can be used at 500 - 800 K.[1,2] It is well known that the properties of TE can be characterized by the figure of merit which is ZT = α2σT/λ, wherein α is the Seebeck coefficient, σ is electrical conductivity, λ is thermal conductivity, and T is the absolute temperature. The figure of

merit (ZT) of PbTe is only 0.8, which can be significantly enhanced via doping with other elements.[3-9]

At present, two kinds of techniques—physical vapor deposition (PVD) and chemical deposition—are used for the preparation of PbTe. Magnetron sputtering,[10] pulsed laser deposition,[11] molecular beam epitaxy (MBE), and thermal evaporation are frequently used in PVD methods.[12,13] However, all PVD technologies involve high temperature or high vacuum, which require professional equipment and strictly controlled experimental conditions. Chemical bath deposition,[14] electrodeposition,[15] electrochemical atomic layer epitaxy (EC-ALE), and solvothermal synthesis are commonly used as chemical techniques for the preparation of PbTe.[16-19] Solvothermal synthesis involves a simple operation, but produces materials with poor mechanical and thermoelectric properties. Therefore, electrodeposition has garnered increasing interest regarding material preparation, due to the advantages of simple preparation, low cost, and easy operation.

PbTe materials can be directly prepared by co-deposition of Pb and Te.[20-32] The effect of substrates on PbTe thermoelectric properties has been emphasized,[20-24] but few studies focus on the formation mechanism of PbTe. Saloniemi group applied an electrochemical quartz crystal microbalance method to study the formation of PbTe in alkaline solutions with TeO_3^{2-} and $PbEDTA^{2-}$.[25] They investigated the effects of reaction time and temperature on product composition of PbTe in NaOH solution.[26] Li and his colleague demonstrated that PbTe was electrodeposited at −0.43 V vs. SCE in HNO_3 solution. [27] Saloniemi had also shown that PbTe could be obtained from aqueous alkaline solutions containing $Pb(CH_3COO)_2$, TeO_2, and disodium ethylenediaminetetraacetate.[15] Wu investigated the PbTe formation process in detail, including the effect of pH value and concentration of Pb(II) and Te(IV).[31] In the study by Frantz, the growth mechanism of PbTe, which included diffusion model and sketches of the growth steps for different morphologies, was determined.[32] Different classifications of electrolyte have also been studied by an electrochemistry approach.[29,30]

However, there are few reported studies on the nucleation mechanism of PbTe in alkaline solution. The influence of applied potential on the concentrations of Pb and Te in coatings and nucleation mechanism have practical implications in fabricating a p-type or n-type of PbTe. The electrochemical behaviors of Pb(II) and Te(IV) in 5 mM $Pb(NO_3)_2$ - 10 mM TeO_2 - 100 mM NaOH solution were studied via cyclic voltammetry on a Cu electrode. The formation and nucleation mechanisms of PbTe were confirmed by chronoamperometry at a potential range from −0.7 V to −1.05 V (vs. Hg/HgO). The results showed that the applied potential was pivotal to the nucleation mechanism and components of deposits.

2. EXPERIMENTAL

Chemicals and reagents (TeO_2 99.99%, NaOH 99.99%, $Pb(NO_3)_2$ 99.999%) were purchased from Alfa Aesar. In electrochemical experiments, a spectral-grade graphite electrode (6 mm in diameter) was used as a counter electrode, while a Cu wire (99.99%, 2 mm in diameter) was employed as a working electrode. A pure Cu plate (99.99%, 2.0 cm^2) was used as the cathode in the electrodeposition experiments. Three kinds of electrolytes (5 mM $Pb(NO_3)_2$ in 100 mM NaOH solution, 10 mM TeO_2 in 100 mM NaOH solution, and 5 mM $Pb(NO_3)_2$ and 10 mM TeO_2 in 100 mM NaOH

solution) were investigated in this study. The pH levels of the three systems were 12.85, 12.97 and 13.22, respectively. All potentials were given with respect to Hg/HgO/NaOH (0.098 V vs. SNE) as a reference electrode (vs. Hg/HgO). Cyclic voltammetry and chronoamperometry methods were applied to investigate the electrochemical behaviors of Pb(II) and Te(IV), and the scan rate was varied from 0.02 V/s to 0.08 V/s. In CV tests, experiments started with an open circuit potential, swept to negative scan, positive scan, and back to starting point. The potential applied in chronoamperometry method was chosen at the reduction peak. The working electrode and the counter electrode were polished with common abrasive paper and metallographic abrasive paper, washed and soaked with acetone, then boiled in 5% dilute hydrochloric acid for 1 h and placed in a glove box. X-ray diffraction (XRD) analysis was performed with X´Pert Pro using Cu K_α radiation, and SEM and EDS investigations were carried out with Ultra Plus. The size and composition of the deposition were measured by EDS.

3. RESULTS AND DISCUSSION

3.1 Cathodic behaviors of Pb in 5mM Pb(NO₃)₂ - 100mM NaOH solution
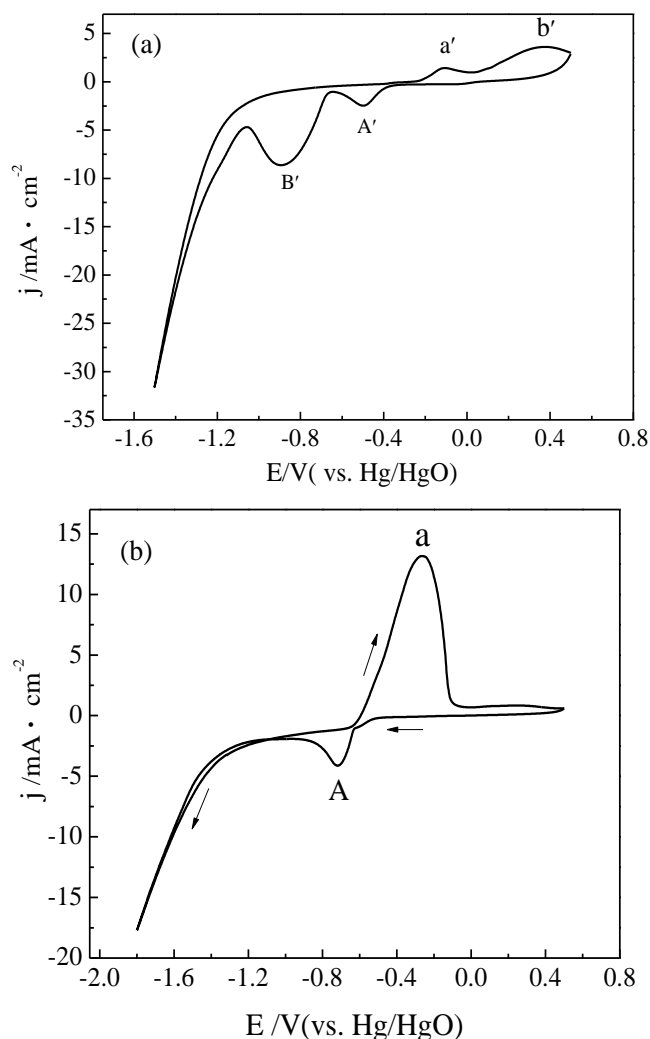
Figure 1. Cyclic voltammograms recorded a: (blank experiment) in solution of 100 mM NaOH, b: in solution of 5mM Pb(NO₃)₂ - 100 mM NaOH at room temperature(WE: Cu, CE: Graphite, RE: Hg/HgO, Scan rate of 0.02 V/s)

To investigate the electrochemical behavior of Pb(II), the cyclic voltammogram (CV), as well as a blank CV curve, were recorded in 5 mM $Pb(NO_3)_2$ - 100 mM NaOH solution and in 100 mM NaOH solution, respectively.

Two waves were observed in the blank curve (Fig. 1, curve a) during the cathodic scan, which indicated that peaks A′ and B′ resulted from the electrochemical reduction of passivating oxide layers on the Cu electrode.[33, 34] From Fig. 1(b), it can be seen that a cathodic current was detected when the potential scans over −0.45 V (vs. Hg/HgO), and peak A at −0.7 V represented a reduction of Pb(II). As the potential shifts to a more negative value, hydrogen evolved from about −1.2 V. During the reverse scan, an oxidation current appeared at −0.6 V and a peak appeared at −0.25 V (peak a), corresponding to the oxidation of Pb. A silver-white film was observed during the cathodic scan so we identified peak A as Pb deposit, and the reduction of Pb(II) is a one step of two- electron process, which is consistent with previous research.[32, 35] While the onset potential of wave A was more positive, this phenomenon was caused by a different presented form of Pb(II) and concentration of Pb(II).[15, 35]

Since the present form of Pb(II) ions in alkaline solution is $HPbO_2^-$,[14] the electrode reaction of peak A can be given by equation (1).

$$HPbO_2^- + 2e^- + H_2O \rightarrow Pb + 3OH^-. \qquad (1)$$

In order to verify the reaction at the potential of peak A, potentiostatic electrolysis was conducted at −0.7 V (vs. Hg/HgO) for 1000 s. The obtained sample was characterized by XRD and SEM as shown in Fig. 2. According to the XRD pattern (Fig. 2(a)), Pb, PbO, Cu, and $NaPb_2(CO_3)_2OH$ were found. Cu was from the working electrode. Because of the weak adherence between Pb and the Cu substrate, we cleaned the electrodeposition. PbO and $NaPb_2(CO_3)_2OH$ were observed, as shown in Fig 2,. PbO came from anode, while $NaPb_2(CO_3)_2OH$ came from the electrolyte which react with CO_2.
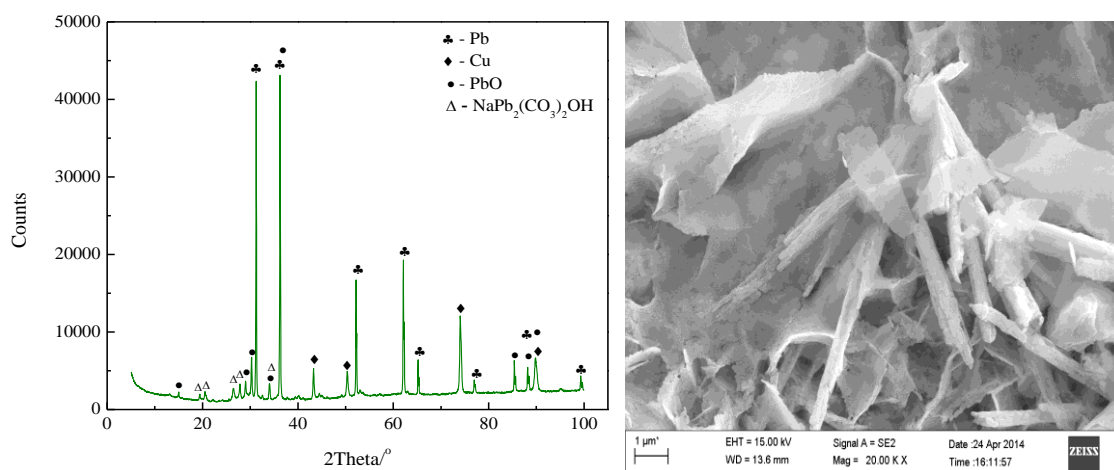
Figure 2. XRD pattern and SEM image of Pb deposit obtained in 5mM $Pb(NO_3)_2$ - 100 mM NaOH electrolyte on Cu substrate for 1000 s.

As mentioned above,[14] Pb(II) species existed as $HPbO_2^-$ in basic solution. During electrodeposition, the anode reaction shown in equation (2) took place and consumed OH^-

continuously, which shifted the reaction (3) to the right and resulted in the continuous formation of PbO.

$$4OH^- - 4e^- = 2H_2O + O_2 \tag{2}$$
$$HPbO_2^- \Leftrightarrow PbO + OH^- \tag{3}$$

When removed the sample from the electrolyte, it absorbed CO_2 from the atmosphere and $Na_2Pb(CO_3)_2OH$ was formed according to equation (4).

$$4NaHPbO_2 + 5\ CO_2 = 2NaPb_2(CO_3)_2OH + Na_2CO_3 + H_2O \tag{4}$$

In addition, SEM image (Fig. 2) indicated that the product was rod-like in shape.

3.2 Cathodic behaviors of Te in 10mMTeO$_2$ - 100mMNaOH solution

As shown in Fig. 3, the electrochemical behavior of Te(IV) in 10mM TeO$_2$ - 100mM NaOH solution was more complicated than Pb(II) due to the high valence of Te(IV).
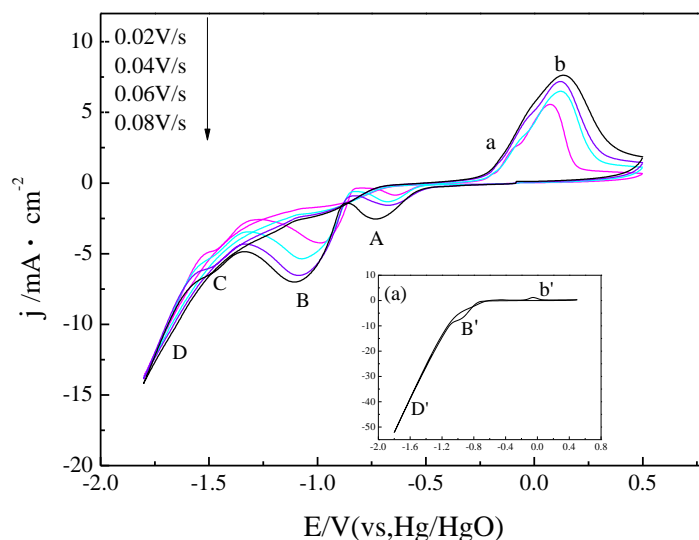
Figure 3. Cyclic voltammogram recorded in 10 mM TeO$_2$ - 100 mM NaOH solution at room temperature on a Cu WE at different scan rates，insert (a) Cyclic voltammogram recorded in 10 mM TeO$_2$ - 100 mM NaOH solution with a scan rate of 0.02 V/s on a Ni WE(CE Graphite, RE Hg/HgO)

Four reduction peaks were observed at a potential of −0.63 V (vs. Hg/HgO, peak A), −0.98 V (peak B), and −1.47 V (peak C). Peak D was identified as hydrogen evolution because of a sharp drop in current and the observed bubble in solution. As the scan rate increased, the reduction peaks potentials shifted to more negative values while the anodic peaks potentials shifted to more positive values, which indicated that the electrochemical reduction of Te(IV) was a quasi- reversible process.

The inset of Fig. 3 shows that only two cathodic current waves (B at −0.97 V and D at −1.16 V) were observed on the Ni electrode in 100 mM NaOH solution. During the reverse scan, the oxidation current waves B' and D' corresponded to the reduction current waves B and D. Due to poor adherence

between the deposited Te and Ni electrode, it was difficult to identify Te deposited on the Ni substrate. Combining the results from Fig. 1, it was concluded that wave A was a result from the Cu substrate (Fig. 1(a)), while waves B and C were related to the reduction of Te(IV). According to some reports,[15, 31] wave B was the reduction of Te(IV) to Te(0), and wave C was caused by the formation of Te^{2-} rather than Te_2^{2-} due to no color change (color of Te_2^{2-} is red). In alkaline solution, TeO_2 can be dissolved in NaOH to form TeO_3^{2-} species by equation (5). Therefore, it was possible to describe peak B and C by equation (6) and equation (7):

$$TeO_2 + 2OH^- \rightarrow TeO_3^{2-} + H_2O \qquad (5)$$
$$TeO_3^{2-} + 3H_2O + 4e^- \rightarrow Te + 6OH^- \qquad (6)$$
$$Te + 2e^- = Te^{2-} \qquad (7)$$
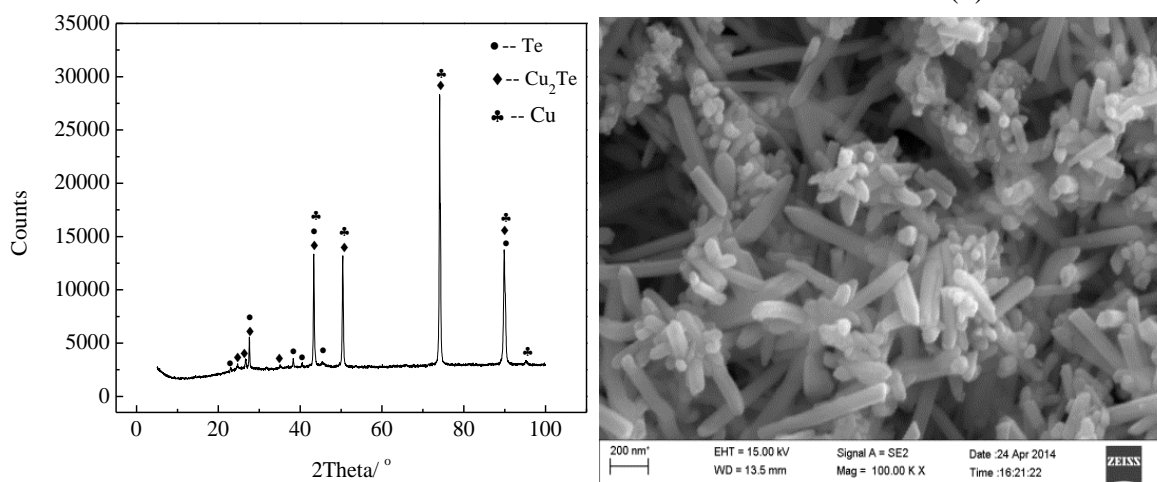
Figure 4. XRD pattern and SEM image of Te deposit obtained in 10mM TeO_2 - 100mM NaOH electrolyte on Cu substrate at –0.98 V for 2000 s.

According to a similar study, the onset potential appeared at −0.74 V vs. Ag/AgCl, while wave B located at −0.86 V (vs. Hg/HgO) in our research which was almost 0.2 V negative than the report. [36] This difference was due to the different pH value and TeO_3^{2-} concentration. Potentiostatic electrolysis was carried out on the Cu electrode at −0.98 V (vs. Hg/HgO). The XRD pattern (Fig. 4) showed that the deposit was composed of pure Te. However, intermetallic compound Cu_2Te was detected by reaction (8) due to the short deposition time and strong formation tendency between deposited Te and Cu substrate corresponded to the analysis of wave A in Fig. 3. Therefore, wave B at −0.97 V in Fig. 3 was identified as the reduction of TeO_3^{2-} to metallic Te.

$$2\,Cu + Te = Cu_2Te \qquad (8)$$

The SEM image in Fig. 4 showed that the Te deposited film was uniform and rod-like with a diameter of 10-50 nm. This size was much smaller than another report where the authors indicated that the shape varied with applied potential and concentration.[36] Therefore, due to a smaller concentration and a much higher pH value, the average size was smaller and rod-like.

3.3 Electrochemical synthesis of PbTe in 10 mM TeO₂ - 5 mM Pb(NO₃)₂ - 100 mM NaOH solution
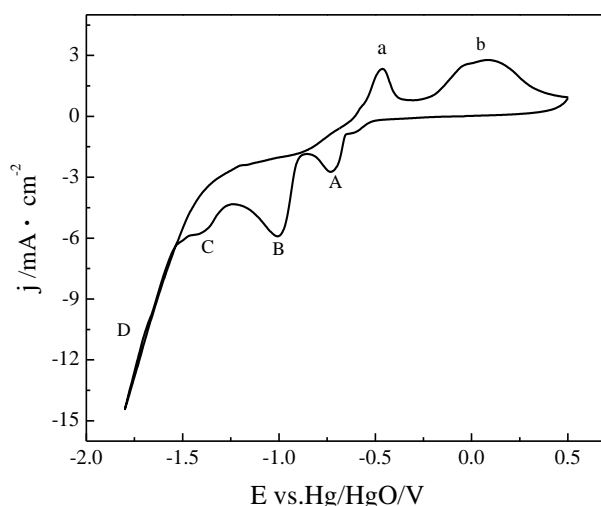
Figure 5. Cyclic voltammogram recorded in TeO_2 - $Pb(NO_3)_2$ - NaOH solution at room temperature. (WE Cu, CE Graphite, RE Hg/HgO, scan rate 0.02 V/s)

The CV curve of the 10 mM TeO₂ - 5 mM Pb(NO₃)₂ - 100 mM NaOH solution (Fig. 5) displays four reduction waves. The most negative reduction current wave D corresponded to hydrogen evolution, while the other three waves were related to the electrochemical reduction of Pb(II) and Te(IV). According to the previous discussion, the peak A at −0.73 V (vs. Hg/HgO) was attributed to the reduction of Pb(II), while peak B at −1.0 V and peak C at −1.38 V were related to the electrochemical reduction of TeO_3^{2-} species. To accurately understand each reduction occurring at the cathode, electrodeposition experiments were conducted at potentials close to the reduction peaks of A, B, and C.
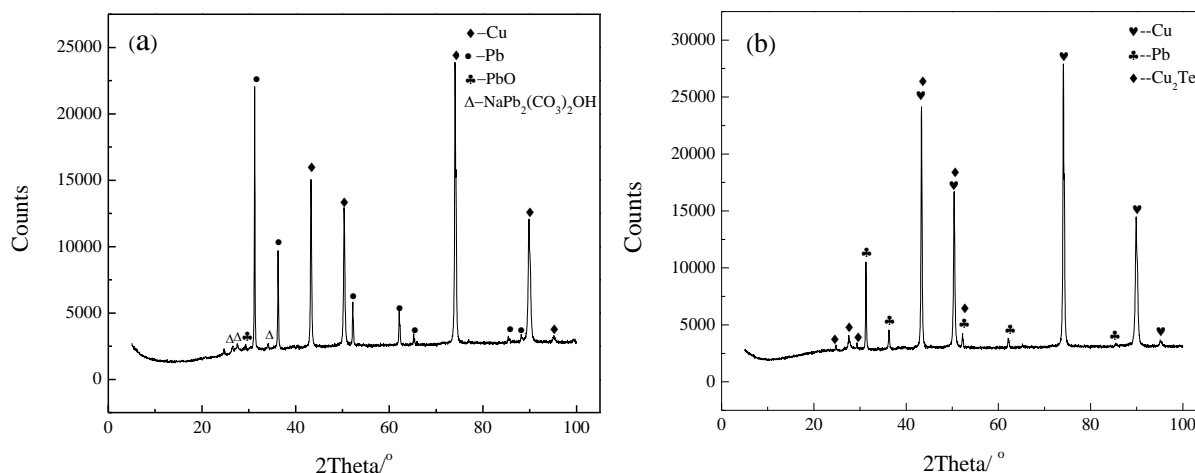
Figure 6. XRD patterns and SEM images of deposits obtained in a 10 mM TeO₂ - 5 mM Pb(NO₃)₂ - 200 mM NaOH solution on a Cu substrate for 2000 s. (a) −0.7 V, (b) −0.9 V.

Deposition at −0.7 V (vs. Hg/HgO) near peak A for 1000 s produced a silver- white film on the working electrode, while some black spots were observed after deposition at −0.9 V for 1000 s. The XRD pattern shown in Fig. 6 (a) demonstrated that the film at −0.7 V was composed of Pb and few PbO, while the deposit obtained at −0.9 V (vs. Hg/HgO) was composed of Pb and Cu_2Te in XRD pattern (Fig. 6 (c)). EDS analysis indicated that the atomic ratio of Pb/Te was nearly 48:52 in the deposit at −0.9 V. However, there was no evidence of PbTe, indicating that there was a stronger tendency to form Cu_2Te than PbTe at a low overpotential. Therefore, a much more negative potential is required to form PbTe.

In addition, electrodeposition experiments were conducted at −0.95 V (vs. Hg/HgO) and −1.05 V around peak B (−1.0 V) for 1000 s. As shown in Fig. 7, a pure film of PbTe was produced based on the XRD pattern and EDS analysis. XRD pattern suggested that the coating was composed of PbTe phase, while EDS analysis showed that the element Pb:Te ratio was 51:49. The potential applied for electro-deposition was almost the same as the potential of peak B in Fig. 3. The reduction peak B in Fig. 3 was associated with the formation of Te, while the reduction peak B in Fig. 5 was due to the co-deposition of Te and Pb. The morphology of PbTe obtained at −0.95 V and −1.05 V was observed by SEM as shown in Fig. 8. PbTe particles prepared at −0.95 V were dense and spherical with a crystal diameter of 100 nm. When deposition potential moves to −1.05 V, agglomeration phenomenon was observed among the particles, and the shape of the particles changed from spherical to leaf-like.
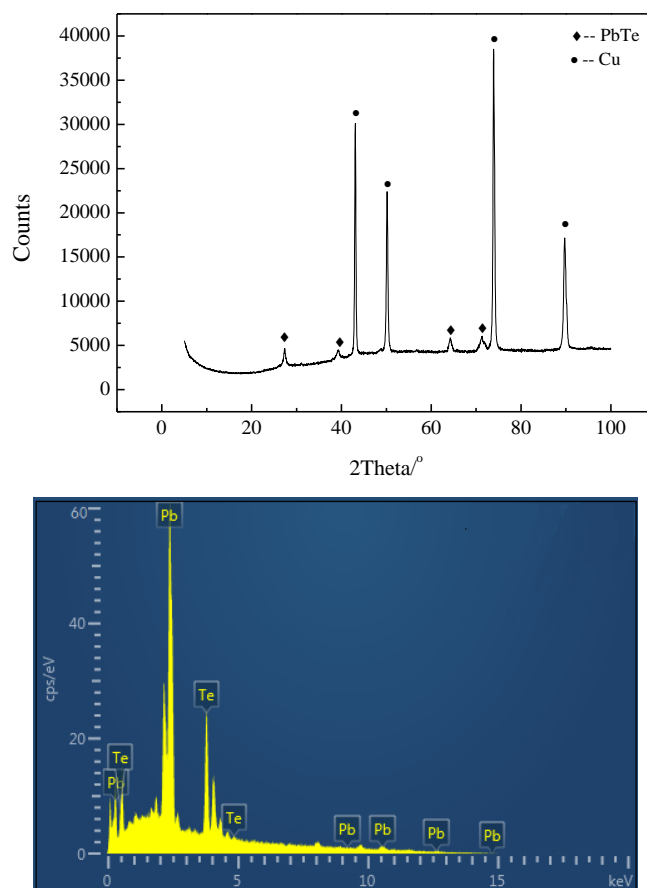
Figure 7. XRD pattern and EDS analysis of PbTe deposit obtained in a 10 mMTeO$_2$ - 5 mM Pb(NO$_3$)$_2$ - 100 mM NaOH solution at –0.95 V and –1.05 V on a Cu substrate.
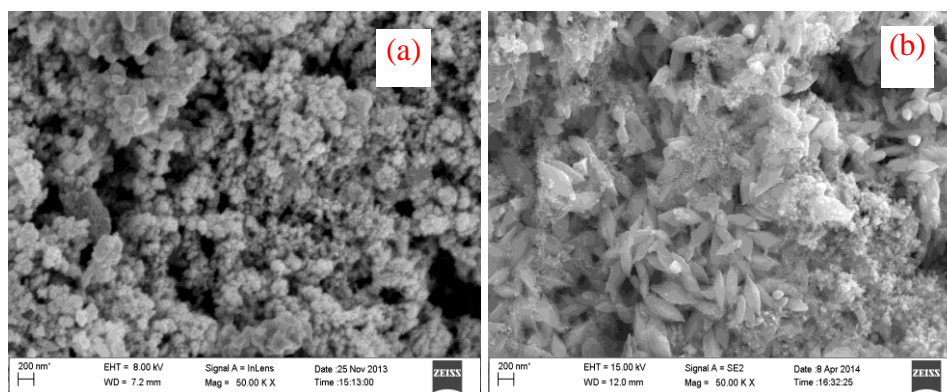
Figure 8. SEM images of a PbTe deposit obtained in a 10 mM TeO_2 - 5 mM $Pb(NO_3)_2$ - 100 mM NaOH electrolyte solution on a Cu substrate. (a) –0.95 V, (b) –1.05 V.

As shown in Fig. 9, the XRD pattern of deposits at −1.15 V (more negative than potential of peak B) illustrated that both Te and PbTe existed, which indicated that Te precipitation has an advantage over Pb at −1.15 V. The EDS analysis indicated that the atomic ratio of Pb/Te was 32:68, which agreed with the XRD pattern. From the results obtained at −0.8 V, −1.05 V, and −1.15 V, it was posited that PbTe was formed by a reaction between metallic Pb and Te, which were already deposited onto a Cu substrate, rather than co-deposition of Pb and Te at the same time. Chronoamperometry experiments were performed at −1.35 V and −1.45 V and there was no solid product obtained on the cathode. However, small bubbles were observed around the electrode surface and disappeared slowly. When electrolysis was carried out at −1.7 V (vs. Hg/HgO), a large amount of gas was produced that did not dissolve. We concluded that the gas evolution at −1.7 V was hydrogen.
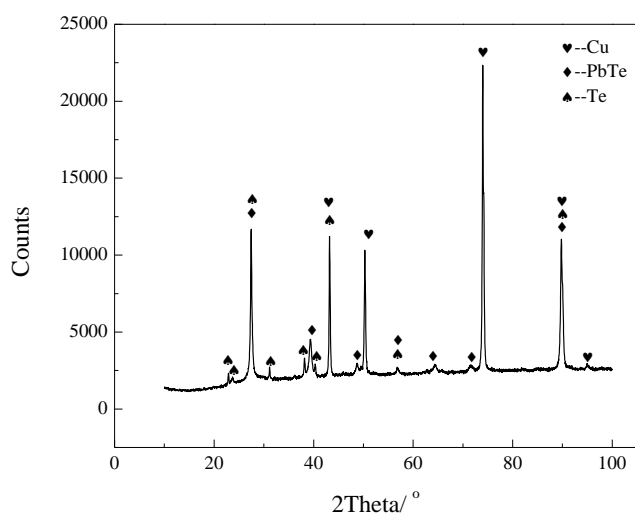
Figure 9. XRD pattern of deposit obtained at –1.15 V in 10 mM TeO_2 - 5 mM $Pb(NO_3)_2$ - 100 mM NaOH electrolyte solution on a Cu substrate.

From Figs. 1, 3, and 5, it was concluded that the shoulder peak at −0.5 V (vs. Hg/HgO) in Fig. 5 was related to Cu substrate, and peak A in Fig. 5 corresponded to the deposition of Pb. Peak B in Fig. 5 was attributed to the formation of PbTe, which resulted from the deposition of Te on the Pb

substrate. Peak C in Fig. 5 was due to the formation of Te^{2-} (Na_2Te), which dissolved into the solution. The onset potential of Pb electrodeposition (−0.66 V) is more negative than the equilibrium potential ($E^{\theta}_{(HPbO2^-)/Pb(0))}$= −0.3759 V),[37] which means that Pb overpotential deposition (OPD) took place on Cu substrate. Xiao demonstrated that when OPD occurred in acidic solution, the content of Pb in PbTe film would exceed 50%.[29] The content of Pb in PbTe film decreased in our study, then increased in a wider range of applied potential. The Wu group investigated PbTe electrochemical behaviors with various parameters and concluded that the PbTe formation was due to an underpotential deposition (UPD) on top of Te, which was different from our result.[31] This opposite conclusion resulted from a different deposition order between Pb and Te; Pb was reduced followed by Te in our study. The electrodeposition of Te and formation of Te^{2-} ions occurred at −0.8 V and −1.26 V, which was different from previous research and the standard electrode potential (−0.67 V and −1.243 V, respectively) due to a different substrate.[15, 38, 39] Compared with the standard electrode potential, the deposition of Te required an overpotential of at least 0.1 V. Based on the above analysis the mechanism of PbTe formation was given by the following equation:

$$TeO_3^{2-} + HPbO_2^- + 6e^- + 4H_2O = PbTe + 9OH^- . \qquad (9)$$

In order to study the nucleation and growth mechanism of Pb and Te, chronoamperometry experiments were carried out in 10 mM TeO_2 - 5 mM $Pb(NO_3)_2$ - 100 mM NaOH solution at -0.7 V, -1.0 V, and -1.15 V(Fig. 10), 5 mM $Pb(NO_3)_2$ - 100 mM NaOH solution at -0.7 V, and 10 mM TeO_2 - 100 mM NaOH solution at −1.0 V(Fig. 11).
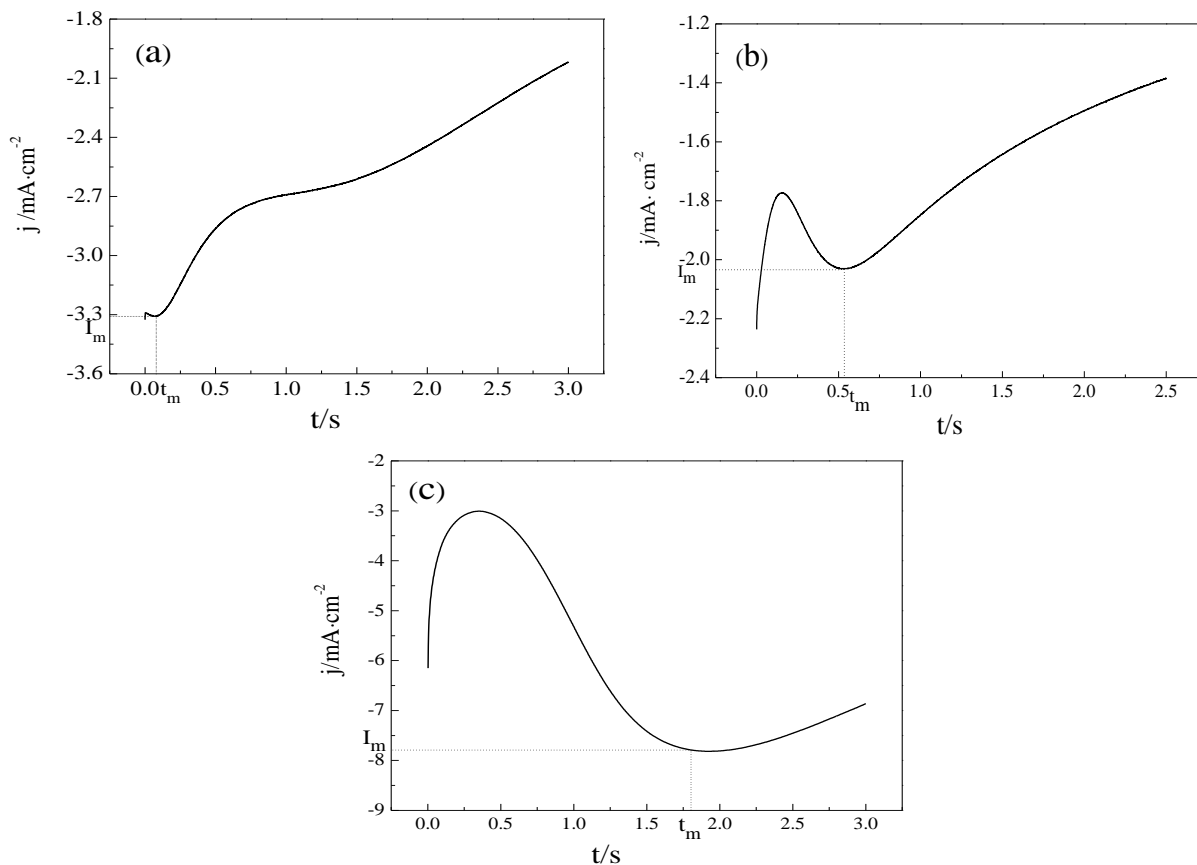
Figure 10. Chronoamperograms recorded on a Cu electrode at various potentials in 5mM $Pb(NO_3)_2$ - 10mM TeO_2 - 100mM NaOH. (a) −0.7 V, (b) −1.0 V, (c) −1.15 V.
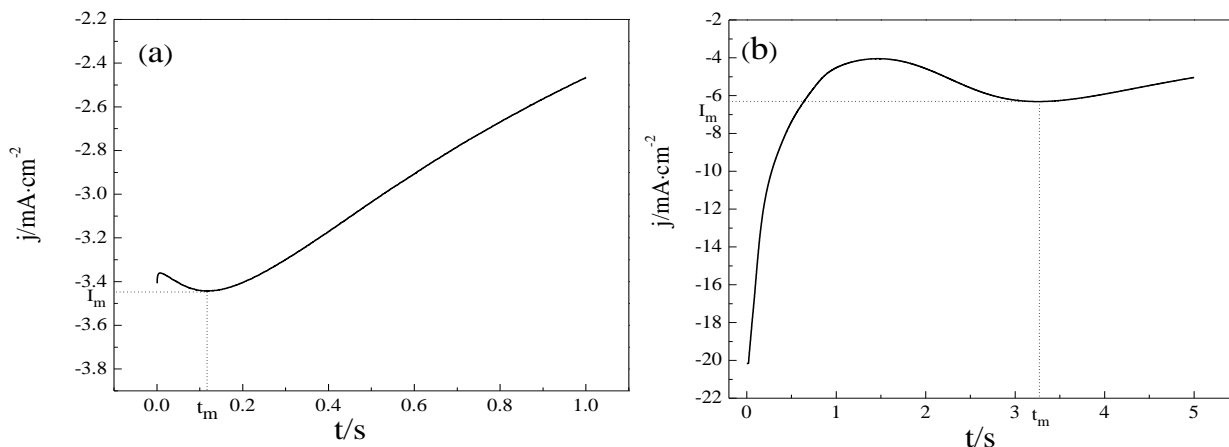
Figure 11. Chronoamperograms recorded on a Cu electrode, (a) −0.7 V in 5mM Pb(NO₃)₂ - 100mM NaOH, (b) −1.0 V in 10mM TeO₂ - 100mM NaOH.

The nucleation mechanism can be classified into 2D instantaneous (2DI), 2D progressive (2DP), 3D instantaneous (3DI), and 3D progressive (3DP) growth. 2D growth mechanism occurs in single-crystal substrates only, and the 2DI nucleation process exhibits a linear relationship between ln (I/t) and t^2, while a 2DP nucleation process exhibits a linear relationship between ln (I/t^2) and t^3. However, as shown in Fig. 12, the experimental results do not fit a 2D growth model because of the nonlinear nature. Therefore, a 3D growth model should be considered. The relationship between $(I/I_m)^2$ and t/t_m was described by equation (10) for 3D instantaneous nucleation and equation (11) for 3D progressive nucleation:

$$(I/I_m)^2 = 1.9542(t/t_m) - 1\{1 - \exp[-1.2564(t/t_m)]\}^2 \tag{10}$$

$$(I/I_m)^2 = 1.2254(t/t_m) - 1\{1 - \exp[-2.3367(t/tm)^2]\}^2 \tag{11}$$
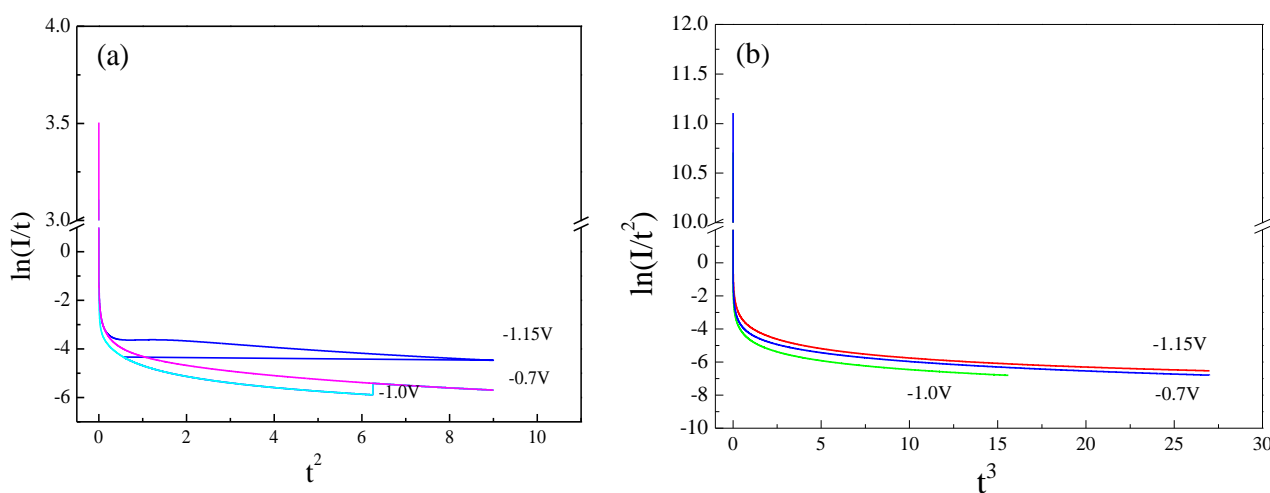
Figure 12. The calculation results for 2D growth mechanism at different potentials, (a) relation between ln(I/t) and t^2 in 2DI, (b) relation between ln(I/t²) and t^3 in 2DP.
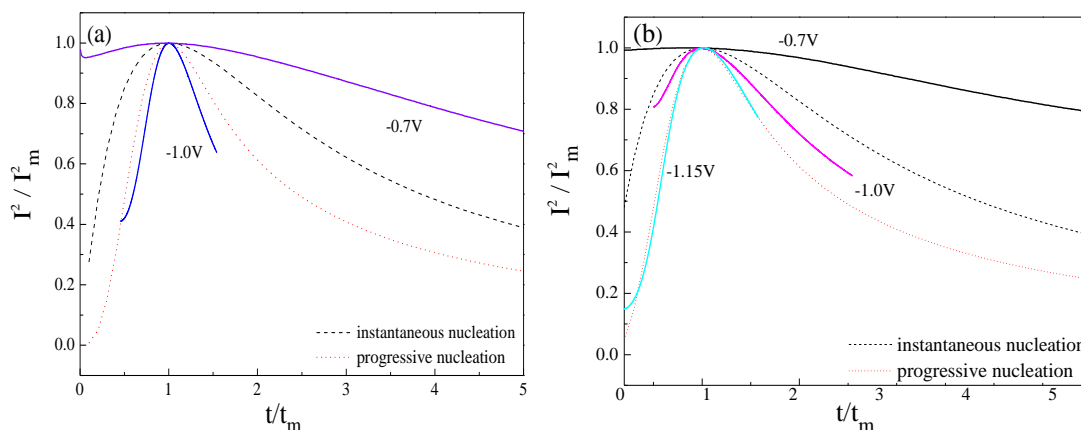
Figure 13. Comparison of the dimensionless curves between theory data and research results, (a) −0.7 V in 5mM Pb(NO$_3$)$_2$ - 100mM NaOH, and −1.0 V in 10mM TeO$_2$ - 100mM NaOH, (b) −0.7 V and −1.0 V in 5mM Pb(NO$_3$)$_2$ - 10mM TeO$_2$ - 100mM NaOH.

Fig. 13 (a) indicates that Pb crystal nucleation agreed well with the instantaneous mechanism at −0.7 V in the 5 mM Pb(NO$_3$)$_2$ - 100 mM NaOH solution, while Te nucleation agrees with a progressive mechanism at −1.0 V in 10 mM TeO$_2$ - 100 mM NaOH solution. Similar 3D instantaneous nucleation processes for Pb deposition were reported in other electrolytes such as urea-EMIC-PbO, urea-BMIC-PbO, and EMI-BF$_4$-PbCl$_2$.[40-42] When experiments were conducted in 5 mM Pb(NO$_3$)$_2$ - 10 mM TeO$_2$ - 100 mM NaOH solution, it was found that PbTe nucleation at −0.7 V fits with instantaneous mechanism, while the nucleation mechanism of PbTe at −1.0 V resulted from instantaneous and progressive mechanisms as shown in Fig. 13 (b). A coating composed of Te and PbTe was obtained at −1.15 V and the nucleation matched well with a progressive mechanism, which was similar to the result of a solution containing Te(IV) as shown in Fig. 13 (a). From the EDS results shown in Fig. 7 and Fig. 9 and a different nucleation mechanism of Pb and Te, it was found that the nucleation mechanism at different potentials corresponded to the dominant electrodeposited element in the mixed system.

It was observed from XRD patterns in Fig. 6 (a), Fig. 7 and Fig. 9 that Pb was obtained at −0.7 V, PbTe can be obtained at −1.0 V, while PbTe and excess Te were obtained at −1.15 V. Te was electrochemically deposited at more negative potential than that of Pb. Combined with the result from Fig. 13, it was concluded that PbTe was formed by a reaction between Pb and Te cathodically. The scheme for electrodeposition of Pb, Te, and PbTe can be summarized as follows:
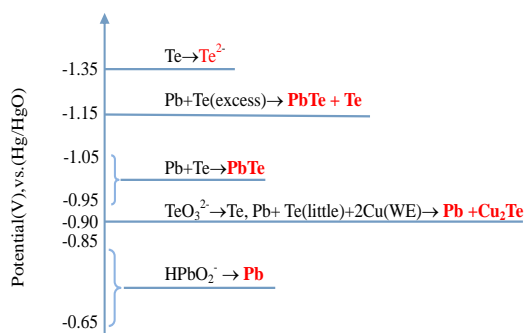
4. CONCLUSION

Electrochemical behaviors and nucleation mechanisms of PbTe in NaOH solution were studied by cyclic voltammetry, chronoamperometry, and electrodeposition experiments at different potentials. CV curves indicated that the reduction of $HPbO_2^-$ occurred at potential more negative than −0.7 V (vs. Hg/HgO), while Te was deposited at a potential between −0.9 V and −1.15 V in an electrolyte containing Pb(II) or Te(IV) species. Based on electrodeposition experiments performed near each cathodic peak in a solution of 5 mM $Pb(NO_3)_2$, 10 mM TeO_2, and 100 mM NaOH, it could be concluded that PbTe was formed at approximately −1.0 V, which was more negative than the potential for the electrodeposition of Pb and Te. The mechanism of PbTe formation can be expressed as TeO_3^{2-} + $HPbO_2^-$ + $6e^-$ + $4H_2O$ = PbTe + $9OH^-$, which resulted from the reaction between Pb and Te that were already deposited on the Cu substrate. When the potential decreased below −1.35 V, metallic Te was reduced to Te^{2-} ions. According to the chronoamperometry experiments, the nucleation and growth mechanism of PbTe at −1.0 V was determined by both instantaneous and progressive mechanisms. Spherical PbTe with a diameter of 100 nm was obtained after electrolysis at −1.0 V for 1000 s. Therefore, it was feasible to electrochemically separate Pb from Te in $Pb(NO_3)_2$ - TeO_2 - NaOH solution, and PbTe intermetallic components with various Te concentration can be obtained by controlling the applied potential.

References

1. M. Hansen，K. Anderko, Constitution of Binary Alloys, McGraw-Hill，NewYork, 1958,1100.
2. Fano V, Lead telluride and its alloys[A], RowE D M，CRC handbook of thermoelectrics [C], London, Press LLC, 1995, 257.
3. http://chemgroups.northwestern.edu/kanatzidis/greatthermo.html.
4. Y. Takagiwa, Y. Pei, G. Pomrehn and G. J. Snyder, *Appl. Phys. Lett.*, 101(2012) 092102.
5. J. R. Sootsman, J. He，V. P. Dravid，S. Ballikaya, D. Vermeulen, C. Uher and M. G. Kanatzidis, *Chem. Mater.*, 22(2010) 869.
6. J. R. Sootsman, H. j. Kong, C. Uher, J. J. D'Angelo, C. I. Wu, T. P. Hogan, T. Caillat and M. G. Kanatzidis, *Angew. Chem.*, 120(2008) 8746.
7. H. K. Fang，L. Sim，G. Fu，C. Wei and J. S. Dyck, *Science* 303(2004) 818.
8. Y. Pei, X. Shi, A. Lalonde, H. Wang, L. Chen and G. J. Snyder, *Nature*, 473(2011) 66.
9. Q. Zhang, F. Cao, W. Liu, K. Lukas, B. Yu, S. Chen, C. Opeil, D. Broido, G. Chen and Z. Ren, *J. Am. Chem. Soc.*, 134(2012) 10031.
10. W. Ren, W. Cao, S. Wang, M. Sui and H. Lu, *J. Alloy Compd.*, 509(2011) 5947.
11. M. Baleva, *Thin Solid Films*, 139 (1986) 71.
12. H. Beyer, J. Nurnus, H. Bo¨ttner, A. Lambrecht, T. Roch and G. Bauer, *Appl. Phys. Lett.*, 80(2002) 1216.

13. A. I. Fedorenko, A. G. Fedorov, A. Y. Sipatov and O. A. Mironov, *Thin Solid Films*, 267(1995) 1347.
14. Y. Y. Wang, K. F. Cai and X. Yao, *J. Solid State Chem.*, 182(2009) 3383.
15. H. Saloniemi, T. Kanniainen, M. Ritala and M. Leskela¨, *Thin Solid Films*, 326 (1998) 78.
16. D. Banga, B. Perdue and J. Stickney, *J. Electroanal. Chem.*, 716(2014) 129.
17. A. Kabalan and P. Singh, *J. Nano Res.*, 31(2015) 30.
18. L. Kungumadevi and R. Sathyamoorthy, *Adv. Powder Technol.*, 24(2013) 218.
19. Q. Yan, H. Chen, W. Zhou, H. H. Hng, F. Y. C. Boey, and J. Ma, *Chem. Mater.*, 20(2008) 6298.
20. R. Madhavaram, J. Sander and Y. X. Gan, *Mater. Chem. Phys.*, 118(2009) 165.
21. Y. A. Ivanova, D. K. Ivanou and E. A. Streltsov, *Electrochem. Commun.*, 9(2007) 599.
22. İbrahim Y. Erdoğan, Tuba Öznülüer, FerhatBülbül and Ümit Demir, *Thin Solid Films*, 517(2009) 5419.
23. D. K. Ivanou, Y.A. Ivanova, A. D. Lisenkov, M. L. Zheludkevich and E. A. Streltsov, *Electrochim. Acta*, 77(2012) 65.
24. J. J. Shi, W. Hu, D. Zhao, T. He and J Zhu, *Sensor. Actuat. B-Chem.*, 173(2012) 239.
25. H. Saloniemi, M. Kemell, M. Ritala and M. Leskela, *J. Electroanal. Chem.*, 482(2000) 139.
26. J. He, S. Mao, S. Zhang, H. Niu, B. Jin and Y. Tian, *Mat. Sci. Semicon. Proc.*, 12(2009) 217.
27. X. Li and I. S. Nandhakumar, *Electrochem. Commun.*, 10 (2008) 363.
28. A. Mondal, N. Mukherjee, S. K. Bhar and D. Banerjee, *Thin Solid Films*, 515(2006) 1255.
29. F. Xiao, B. Yoo , M. A. Ryan , K. H. Lee and N. V. Myung, *Electrochim. Acta*, 52(2006) 1101.
30. Y. Y. Feng and M. Gu, *Electrochim. Acta*, 90(2013) 416.
31. C. Frantz, Y. Zhang, J. Michler and L. Philippe, *CrystEngComm*, 18(2016)2319.
32. T. Wu, H. Lee and N. V. Myung, *J. Electrochem. Soc.*, 163(2016)D801.
33. J. G. Becera, R. C. Salvarezza and A. J. Arvia, *Electrochim. Acta*, 33 (1988) 613.
34. D. D. La, S. Y. Park, Y. W. Choi and Y. S. Kim, *B. Kor. Chem. Soc.*, 31(2010) 2283.
35. C. Frantz, C. Vichery, J. Michler and L. Philippe, *Electrochim. Acta*, 173(2015)490.
36. T. Wu, M. Zhang, K. Lee, C. Lee, H. Lee, Y. Choa and Nosang V. Myung, *J. Electrochem. Soc.*, 164(2017)D82.
37. P. Atkins, Physical Chemistry, 6th edition, W.H. Freeman and Company, New York, 1997.
38. Z. Yao, M. Liu, P. Zhang, X. H. He, G. R. Li, W. X. Zhao, P. Liu and Y. X. Tong, *Electrochim. Acta*, 54(2008) 247.
39. A. J. Bard, R. Parsons and J. Jordan, Standard Potentials in Aqueous Solutions, Marcel Dekker, New York, 1985.
40. R.W. Tsai, Y.T. Hsieh, P.Y. Chen, and I. W. Sun, *Electrochim. Acta*, 137 (2014) 49.
41. W.C. He, A.M. Liu, J.Z. Guan, Z.N. Shi, B. L. Gao, X. W. Hu, and Z.W. Wang, *RSC Adv.*, 7 (2017) 6902.
42. Liu, Aimin, Zhongning Shi, and Ramana G. Reddy, *Electrochim. Acta* (2017). https://doi.org/10.1016/j.electacta.2017.08.011.